Int. J. Heat Mass Transfer. Vol. 26, No. 8, pp. 1109–1120
Printed in Great Britain

0017-9310/83 $3.00 + 0.00
Pergamon Press Ltd.

HIGH TEMPERATURE CATALYTIC COMBUSTION OF CO–O_2–N_2, Ar, He, CO_2–H_2O MIXTURES OF PLATINUM

C. BRUNO
Princeton Combustion Research Labs, Princeton, New Jersey, U.S.A.

P. M. WALSH
Energy Laboratory, Massachusetts Institute of Technology, Cambridge, Massachusetts, U.S.A.

and

D. SANTAVICCA and F. V. BRACCO
Mechanical and Aerospace Engineering Department, Princeton University, Princeton, NJ 08544, U.S.A.

(*Received* 2 *March* 1982 *and in revised form* 23 *September* 1982)

Abstract—In a steady flow reactor, using a platinum-coated honeycomb catalyst with channel diameter of 1.4 mm and length of 76 mm, measurements were made of substrate temperature at ten axial locations, exhaust concentrations of CO, CO_2, O_2 and pressure drop with CO–air mixtures at 600 K inlet temperature, 110–200 kPa pressures, 10–70 m s^{-1} inlet velocities, 0.013–0.32 equivalence ratios, and 0.54 mol% water content. Also employed were CO–CO_2, N_2, Ar, He–O_2 mixtures at 600–700 K, 110 kPa, 11–13 m s^{-1}, and 0.031–0.56 equivalence ratios. The gas processes within a channel were then computed with a 2-dim. steady state model that includes axial and radial convection, laminar diffusion of mass, momentum and energy, a homogeneous single step irreversible reaction and, initially, a finite-rate surface reaction. Comparison of computed and measured quantities is satisfactory. Under the conditions tested, oxidation of CO is mostly diffusion-controlled. Homogeneous reactions are important only for the lowest velocities and highest equivalence ratios. It would appear that the presence of water increases the rate of high temperature catalytic oxidation of CO.

NOMENCLATURE

C_p, gas specific heat;
$D = D_h$; hydraulic diameter;
D_{ik}, binary diffusion coefficient for species i, k;
E, activation energy;
k, thermal conductivity;
p, pressure;
r, channel radial coordinate;
R, channel radius; universal gas constant;
Re, Reynolds number;
S_ϕ, source term in generalized conservation equation;
t, time;
T, gas temperature;
u, axial gas velocity component;
v, radial gas velocity component;
x, channel axial coordinate;
X_k, molar fraction of species k;
Y_k, mass fraction of species k;
W_k, molecular weight of species k.

Greek symbols

Γ, gas transport property in generalized conservation equation;
λ, gas thermal conductivity;
μ, gas viscosity;
ρ, gas density;
ϕ, equivalence ratio $= (Y_{CO}/Y_{O_2})/(Y_{CO}/Y_{O_2})_{Stoich}$. Also general dependent variable of the gas phase conservation equations.

Subscripts

$()_{in} = ()_2$, at the channel inlet;
$()_w$, at the wall.

1. INTRODUCTION

THE TECHNOLOGY and data base needed to incorporate catalytic reactors in practical heat and power systems are expanding rapidly. The work in progress includes development of catalytic combustors for aircraft gas turbines [1–6], stationary gas turbines [7–12], highway vehicle gas turbines [13–17], and boilers [10]. Other studies have focused on catalyst design for particular fuels such as low-Btu gases [18], No. 6 oil [19], heavy fuels [20], and coal-derived liquids [21]. Still other work has been concerned with catalyst durability [22]. Demonstrated advantages of catalytic, when compared with conventional, combustion are lower emissions of hydrocarbons, CO, NO_x and smoke, higher efficiency, stable operation at lower equivalence ratio, improved pattern factor (for gas turbines) and use of fuels of wider specification. Potential for low conversion of fuel-bound nitrogen to NO_x has also been demonstrated [19, 23–25]. Further development and optimization could be facilitated by better knowledge of the processes which control fuel conversion in the channels of a monolithic catalyst.

A number of physical and chemical processes have been suggested as important determinants of steady catalytic combustor performance [27–29], namely axial and radial convection of species, heat, and momentum, axial and radial diffusion of species, heat,

and momentum, axial heat transfer in substrate by conduction and radiation, gas and wall chemical reactions, but only some of them have been considered in published work.

Cerkanowicz, Cole, and Stevens [30] modeled the steady state operation of a catalyst including one-step homogeneous and heterogeneous reactions, radial heat and mass transport, axial heat conduction in the solid, and axial variation in pressure and flow velocity. They assumed plug flow and constant transfer coefficients. The results were compared with the experimental data of Pfefferle *et al.* [7] on the catalytic combustion of propene. The model successfully predicted the transition from surface reaction to diffusion control, and the initiation of homogeneous reactions, as inlet temperature increases. It also correctly predicted the equivalence ratio at which homogeneous reaction is initiated with fixed inlet temperature. The model exhibited ignition–extinction hysteresis, which has also been observed experimentally.

Kelly *et al.* [28] modeled steady state operation using multiple homogeneous reactions, one-step wall reaction, axial heat and species diffusion, and axial substrate heat transfer by conduction and radiation. Flow velocity was variable, but pressure was fixed. Radial transport was treated using variable transfer coefficients. Studies with this model showed that a distinct light-off transition for homogeneous reactions depends on the inclusion of axial diffusion of both heat and species. The model predicted that both blowout mass throughput and emissions increase with increasing channel diameter. These observations led to the development of graded cell catalysts with improved performance [31].

T'ien [32] modeled 1-dim. steady state operation in a fashion similar to Kelly *et al.*, but neglecting axial conduction and radiative heat transfer in the substrate. He concentrated on the effects of catalyst length on fuel conversion.

In the above three approaches, the channel flow was treated as 1-dim. thus excluding the resolution of radial gradients and requiring the use of global transfer coefficients. Also, interactions of radial diffusion and homogeneous and heterogeneous reactions are accounted for very roughly in 1-dim. descriptions. In this paper results of 2-dim. computations of the homogeneous and heterogeneous oxidation of CO in air over a platinum catalyst and comparisons with measured CO emissions vs inlet pressure, temperature, equivalence ratio, and velocity are reported.

From the point of view of applications, the oxidation of CO has long been known to be important in the homogeneous combustion of hydrocarbons [33], while the choice of platinum is due to its low light-off temperature, ease of fabrication, and the existence of a substantial body of knowledge about its performance in the oxidation of CO, albeit at lower temperatures. Its high cost and short high-temperature life, however, make it an unlikely candidate for most high-temperature applications for which cheaper and more stable catalysts are being designed and evaluated.

2. EXPERIMENTAL APPARATUS

2.1. *Test rig*

A sketch of the experimental apparatus is shown in Fig. 1. Pre-heated air at a measured flowrate is supplied to a 690 mm long test section with a 25.4 mm square cross section channel. The catalyst is placed with its downstream end 90 mm from the test section outlet, and insulated from the wall by Fiberfrax paper. Details of the catalyst section are shown in Fig. 2. A fuel injector consisting of five 1.6 mm diameter tubes, each containing five 0.3 mm diameter holes, is located 440

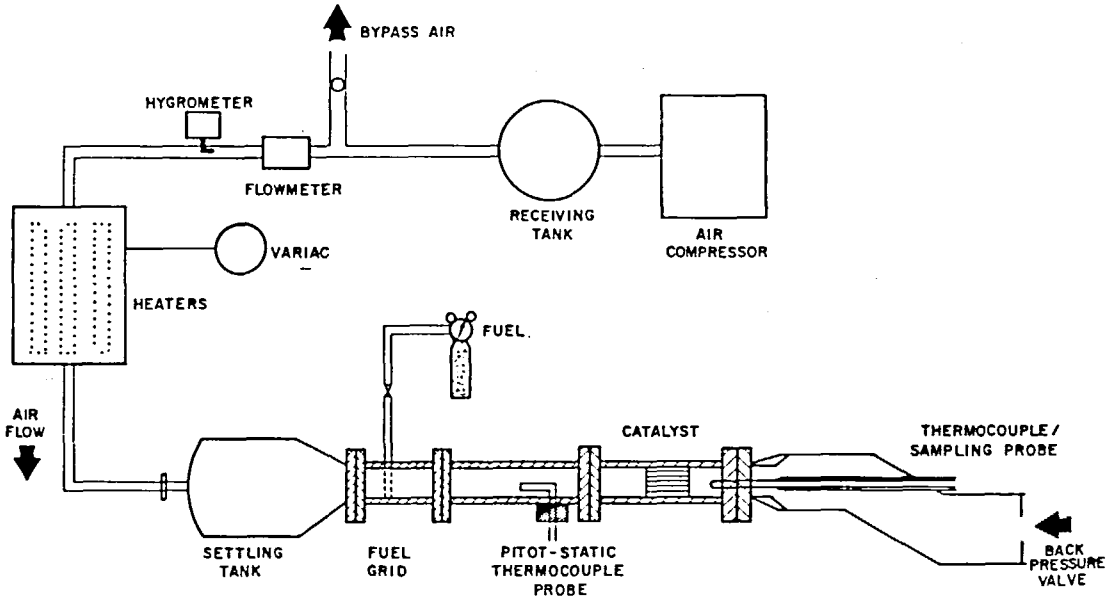

FIG. 1. Schematic diagram of the flow reactor with catalytic combustion test section.

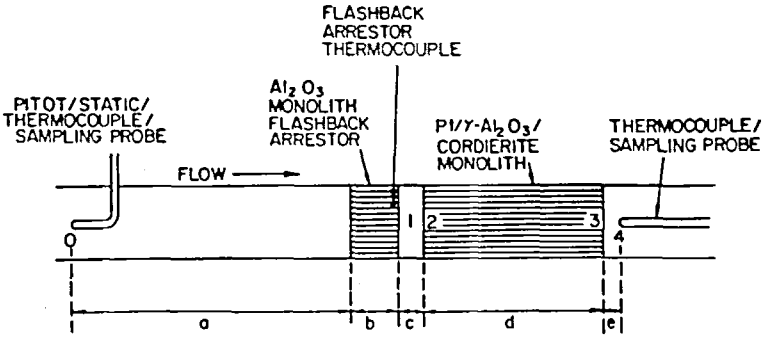

a 0.217 ± 0.001 m
b 0.0132 OR 0.0262 ± 0.0003 OR 0
c 0.001 TO 0.003
d 0.0760 ± 0.0003
e 0.0010 ± 0.0005

FIG. 2. Details of the catalyst test section.

mm from the catalyst inlet. A combination pitot tube and thermocouple is mounted 233 mm from the catalyst inlet. In addition to measuring gas velocity and temperature, the pitot tube is used to extract gas samples which are analyzed to determine the equivalence ratio. Pressure is regulated by a valve in the exhaust pipe, and taps placed up and downstream of the catalyst are used to measure inlet pressure and pressure drop. A mass flowmeter (Hastings Model AHL-100P with H-3M/L-100 Transducer) measured the air flowrate. The water content of the inlet air was measured using a semiconductor sensor (Thunder Model 2000 with BR-101B probe) mounted in the airstream between the receiving tank and the heaters.

Efforts were made to minimize crosswise gradients in temperature, velocity, and fuel concentration of the inlet stream. The entire test section is insulated and a temperature gradient of less than 10 K/channel across the width of the test section is obtained when sufficient time (~1 h) is allowed after startup of the air preheat system. The uniformity is found to be independent of air flowrate over the range of velocities used. Sufficient fuel–air mixing was obtained by careful design of a fuel injection grid constituted by an array of vertical tubes. Equally-spaced holes were drilled into the tubes so as to produce fuel jets parallel to the airstream. The resulting fuel distribution showed good uniformity (±3%) over the measured range. Velocity profiles were less satisfactory (range ±6% over 50% of the channel width). Average reference velocities were determined using the CO and air flowrates, inlet temperature and pressure, and the cross section area of the catalyst. The catalyst channel inlet velocity, taking into account the fraction of open monolith area, is $u_{in} = (1.67 \pm 0.06)u_{ref}$.

2.2. *Substrate and exhaust measurements*

Substrate temperatures were measured by a method similar to that described by Hegedus [34] and Kesselring *et al.* [31]. Ni–Cr/Ni–Al thermocouples were fed through the test section wall and into the front end of the catalyst channels. Pt/Pt–Rh thermocouples were similarly used from the back end. The lengths of wire inside the catalyst were covered by mullite insulator and both ends of the channel sealed with ceramic adhesive. The temperature measurements were made in channels around the central one. Exhaust gas samples were taken through an expansion quenched, water cooled, stainless steel probe mounted in an elbow downstream of the test section. The entrance of the probe was aligned with the central channel. Exhaust gas temperature was measured with a Pt/Pt–Rh thermocouple, coated with silica, mounted on the probe. CO and CO_2 were determined by infrared absorption (Horiba Model AIA-21), and O_2 by magnetic susceptibility (Scott Model 250).

2.3. *Catalyst and fuel*

The catalyst was platinum supported on split cell corrugated Cordierite with γ-alumina washcoat. The overall dimensions of the monolith were 24 × 24 × 76 mm, the open area was 64%, the channel cross-section area was 1.9 mm^2, and the platinum loading was 4.2 kg m^{-3}. The physical properties of the catalyst are listed in Table 1. The fuel was carbon monoxide, C.P.99.5 mol % min.

3. MATHEMATICAL MODEL

Only the central channel of the catalytic monolith was modeled. The wall temperature, obtained from the wall thermocouple measurements, was specified as a function of x over the entire length of the channel. This procedure tests the validity of the gas-phase model more strictly by separating gas-phase from substrate effects [35], and has the additional advantage of implicitly including radiative heat transfer (provided the gas is optically thin) and heat losses across the width of the monolith. Indeed the actual, measured wall

Table 1. Catalyst properties

Substrate: Cordierite, American Lava Corp., AlSiMg 795, split cell
- length 0.0760 ± 0.003 m
- wall thickness 0.25×10^{-3} m
- open area 64%
- channels per unit area 0.35×10^{6} m^{-2}
- open area per channel 1.9×10^{-6} m^{2}
- ratio surface area to total volume 2100 m^{-1}
- ratio surface area to gas volume 3260 m^{-1}
- channel hydraulic diameter 0.0014 m
- bulk density 610 kg m^{-3}
- solid density 1700 kg m^{-3}
- safe operating temperature 1473 K
- specific heat 800 J kg^{-1} K^{-1}
- coefficient of thermal expansion (linear, 294–1033 K) 3.8×10^{-6} K^{-1}
- thermal conductivity of solid (572 K) 1.4 J m^{-1} s^{-1} K^{-1}
- approximate channel cross section is a trapezoid with base lengths 0.0011 m and 0.0023 m, and height 0.0012 m

Washcoat: γ-alumina
- loading 115–125 kg m^{-3}
- surface area (BET) $(29.2–33.0) \times 10^{6}$ m^{-1}

Catalyst: platinum
- loading 4.2 kg m^{-3}
- surface area (CO chemisorption) 6×10^{4} m^{-1}
- (The γ-alumina and platinum were applied by Matthey Bishop Inc., Malvern, PA.)

temperature includes all those effects. Since the embedded thermocouples and the combination thermocouple/sample probe measured quantities related to the central channels, errors due to the small cross section non-uniformities were minimized.

Axial symmetry was assumed in modeling the individual channel, whose cross section is roughly trapezoidal. The diameter of the model channel was chosen as the hydraulic diameter, $D_h = 4 \times$ area/perimeter. For the monolith used in the present work $D_h = 1.4$ mm.

3.1. *Gas equations*

The equations for the gas inside each channel are the complete, steady, 2-dim. conservation equations for reactive, laminar ($Re < 1900$) flows [36]. They were solved numerically by a method based on the TEACH code documented by Gosman and Ideriah [37]. The code used in the present work differs significantly from the original TEACH, written for incompressible nonreactive flows, due to the introduction of variable density, of species and energy conservation equations, and of the equation of state, linking pressure, density and species mass fractions.

In this code the general conservation equation is written as

$$\frac{1}{r}\left[\frac{\partial}{\partial x}(\rho r u\phi)+\frac{\partial}{\partial r}(\rho r v\phi)-\frac{\partial}{\partial x}\times\left(r\Gamma\frac{\partial\phi}{\partial x}\right)-\frac{\partial}{\partial r}\left(r\Gamma\frac{\partial\phi}{\partial r}\right)\right]=S_\phi \quad (1)$$

where $\phi \equiv u, v, T, Y_k$, etc.; Γ is the appropriate transport property, such as μ, k, ρD_{ik}, and S_ϕ is the appropriate source term, such as $-\partial p/\partial x$, or the rate of formation for the species equations. The transport coefficients are temperature dependent and were obtained from ref. [38].

The general equation is integrated over the elemental cell volume, so that only convective and diffusive fluxes, and sources appear in the algorithm. The resulting finite difference equations are linear and are solved iteratively. To this purpose the integration domain is divided into mesh subdomains (cells) and the code solver computes for each variable a new line of values at each longitudinal location x. After the entire mesh has been swept, the code computes the total amount of the quantities to be conserved, compares them to the fluxes entering the inlet of the monolith channel and keeps iterating if the percentage difference is above a specified value, typically 0.5%. Further details may be found in ref. [37].

The model chosen for the homogeneous kinetics of CO with O_2 is a simple, one-step overall reaction CO $+(1/2)\,O_2 \rightarrow CO_2$. The rate was taken from ref. [39]

$$\frac{d[CO]}{dt} = -k_0[CO][O_2]^{0.5}[H_2O]^{0.5}\exp(-E/RT) \quad (2)$$

with

$$k_0 = 1.3 \times 10^{14}\ \text{cm}^3\ \text{mol}^{-1}\ \text{s}^{-1}$$

and

$$E = 126\ \text{kJ mol}^{-1} = 30\ \text{kcal mol}^{-1}.$$

3.2 *Gas boundary conditions*

At the inlet ($x = 0$) all physical variables ϕ are assumed to be known. At the outlet ($x = L$) their gradients are set to zero: $\partial\phi/\partial x = 0$. This condition simplifies the solution, and is also observed in practice, provided the L/D ratio of the channel is sufficiently large. Tests with imposed, arbitrary, large $(\partial\phi/\partial x)_{x=L}$ did not show any detectable effect on the results except very near the outlet itself.

The other boundary conditions express radial symmetry, i.e. $\partial\phi/\partial r = 0$ at $r = 0$. At the channel wall, $r = R$, no-slip conditions apply to u, v, and the measured temperature was used as explained earlier.

The species N_2 and H_2O are assumed inert, and their radial gradients zero at $r = R$. Initially heterogeneous kinetics rates were used for CO at the wall, and the following balance of diffusion and reaction rates imposed

$$\rho D_{CO,N_2}\frac{\partial Y_{CO}}{\partial r} = -A_w\rho Y_{CO}\exp(-E_w/RT_w) \quad (3)$$

where $A_w = 3.82 \times 10^3$ m s^{-1}, $E_w = 104.25$ kJ mol^{-1} $= 24.9$ kcal mol^{-1} were obtained from ref. [40]. Further assuming that at the wall CO is oxidized via the reaction $CO + O_2/2 \rightarrow CO_2$, the boundary conditions

for O_2 and CO_2 at $r = R$ were written as

$$\frac{\partial Y_{O_2}}{\partial r} = \frac{1}{2}\frac{\partial Y_{CO}}{\partial r}\frac{W_{O_2}}{W_{CO}}\frac{D_{CO,N_2}}{D_{O_2,N_2}},$$

$$\frac{\partial Y_{CO_2}}{\partial r} = -\frac{\partial Y_{CO}}{\partial r}\frac{W_{CO_2}}{W_{CO}}\frac{D_{CO,N_2}}{D_{O_2,N_2}}.$$

However, no accurate matching between computed and measured data could be obtained using this heterogeneous rate. Much better agreement was achieved by increasing A_w by $O(10^3)$ and refining the computational mesh by a factor of 2 in both directions. (Finer mesh is necessary when some terms, such as kinetic rates, are increased, to compensate for the inevitable averaging associated with finite differencing.) Further reduction of the mesh size changed the results only slightly.

Clearly, the rate given in ref. [40] for automotive exhaust catalytic converters, applies in a temperature regime much lower than the one of interest in this study. Since the larger A_w resulted in very low CO mass fractions at the wall, indicating that conversion was diffusion controlled, the heterogeneous CO rate ultimately was assumed infinitely fast, with insignificant changes in the results, and the boundary condition for CO changed to

$$(Y_{CO})_{r=R} = 0$$

while the conditions for O_2 and CO_2 were unchanged. Notice that very fast heterogeneous reactions in steady state do not imply in any way a similar condition during the ignition transient. Indeed the initial light-off at the entrance of the catalyst is controlled by heterogeneous kinetics.

4. RESULTS

4.1. CO–*air mixtures*

A total of 78 tests were performed. The results are given in the figures. The main inlet conditions were:

Inlet temperature (T_{in}) = 600±10 K,
Inlet pressure (P_{in}) = 110±5 kPa and 200±7 kPa,
Inlet velocity (u_{in}) = 10±4 to 70±9 m s^{-1},
CO-air equivalence ratio (ϕ) = 0.003±0.006 to 0.32 ±0.07,
H_2O = 0.54±0.07 mol %.

Analysis of the computed $\Delta p/p$ across the monolith indicates that the hydraulic diameter choice $2R = 1.4$ mm reproduces the experimental data at both $p = 110$ and $p = 200$ kPa. Trends are as expected, with $\Delta p/p$ increasing with velocity and ϕ, due to increases of the velocity gradient at the wall and of the viscosity (Figs. 3 and 4).

A sample of measured wall temperature profiles is shown in Fig. 5. At the same equivalence ratio there is hardly any effect of velocity or pressure, meaning that the wall temperature is very close to the adiabatic flame temperature. If the Lewis number is also close to unity, then the implication is that the process is diffusion-controlled. Emissions, in terms of $X_{CO}/(X_{CO}+X_{CO_2})$ at the outlet, i.e. in terms of unburnt carbon, are plotted vs ϕ in Figs. 6 and 7. The model predicts emissions well in the middle-to-high velocity range, while it is less satisfactory when the velocity is low.

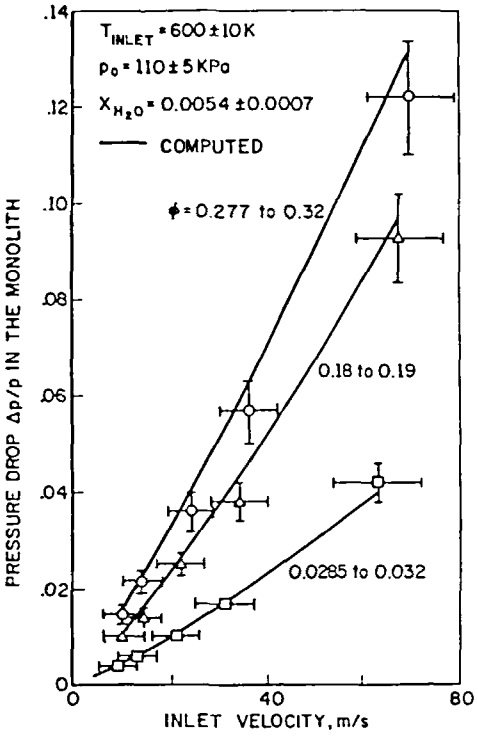

FIG. 3. Measured and computed pressure drop vs inlet velocity and equivalence ratio at specified inlet temperature, pressure and water content.

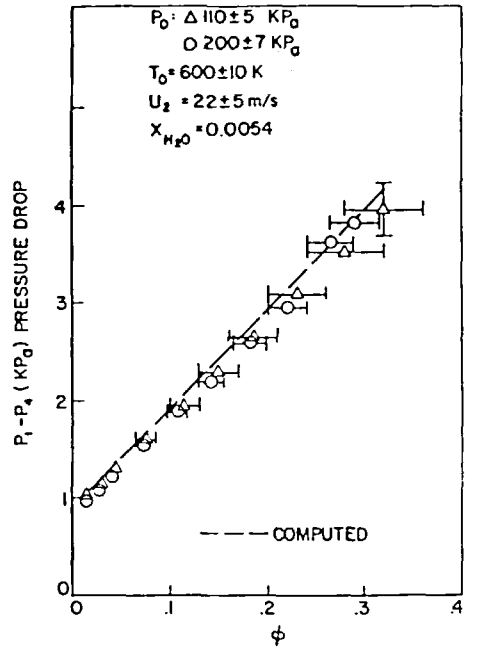

FIG. 4. Measured and computed pressure drop vs equivalence ratio at specified inlet temperature, pressure, velocity and water content.

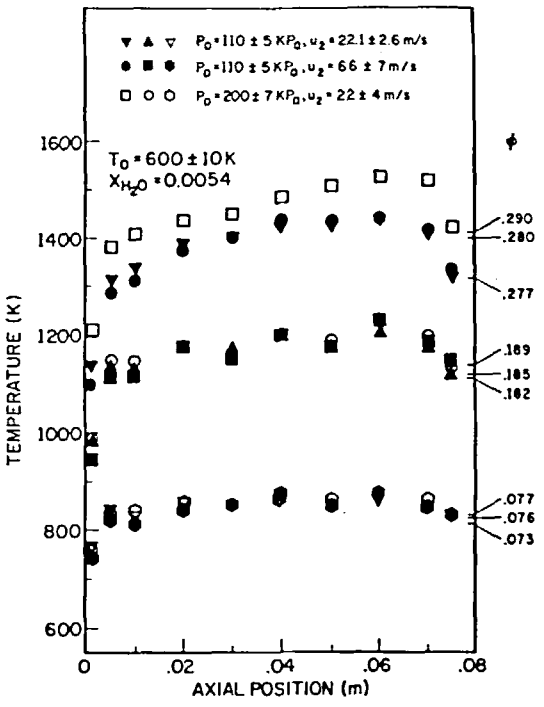

FIG. 5. Measured substrate temperature as a function of axial position, equivalence ratio, pressure and velocity.

Figure 6 shows the main features of CO oxidation. At constant velocity, for sufficiently small values of ϕ the amount of oxidized CO is minute and the emission parameter $X_{CO}/(X_{CO}+X_{CO_2})$ tends to unity. As ϕ is slightly increased, catalytic reactions begin, and emissions decrease rapidly. This regime, where the fuel diffusing to the wall is oxidized at a finite rate (of the type suggested by Voltz *et al.* [40]), is the heterogeneous-kinetics controlled regime.

Increasing ϕ further accelerates the wall reaction(s), until they become as fast, or faster, than the rate of diffusional transport to the wall. At this point the regime becomes diffusion-controlled, as shown by an invariance of the emission parameter with ϕ. This flat part of the emission curves is broader at higher flow velocities (short residence time) and becomes very narrow (in fact, barely noticeable) for long residence times.

Eventually, as ϕ is further increased, more and more CO is oxidized in the gas phase, and emissions decrease rapidly controlled by homogeneous-kinetics rates.

Increasing or reducing the flow velocity alters events quantitatively but not qualitatively. In particular, the emission plateau corresponding to the pure diffusion-controlled regime broadens as the velocity is increased, until, when the velocity is infinitely large, it occupies the entire ϕ range and no oxidation occurs, i.e. $X_{CO}/(X_{CO}+X_{CO_2})=1$.

The effect of pressure can be observed in Fig. 7. Since

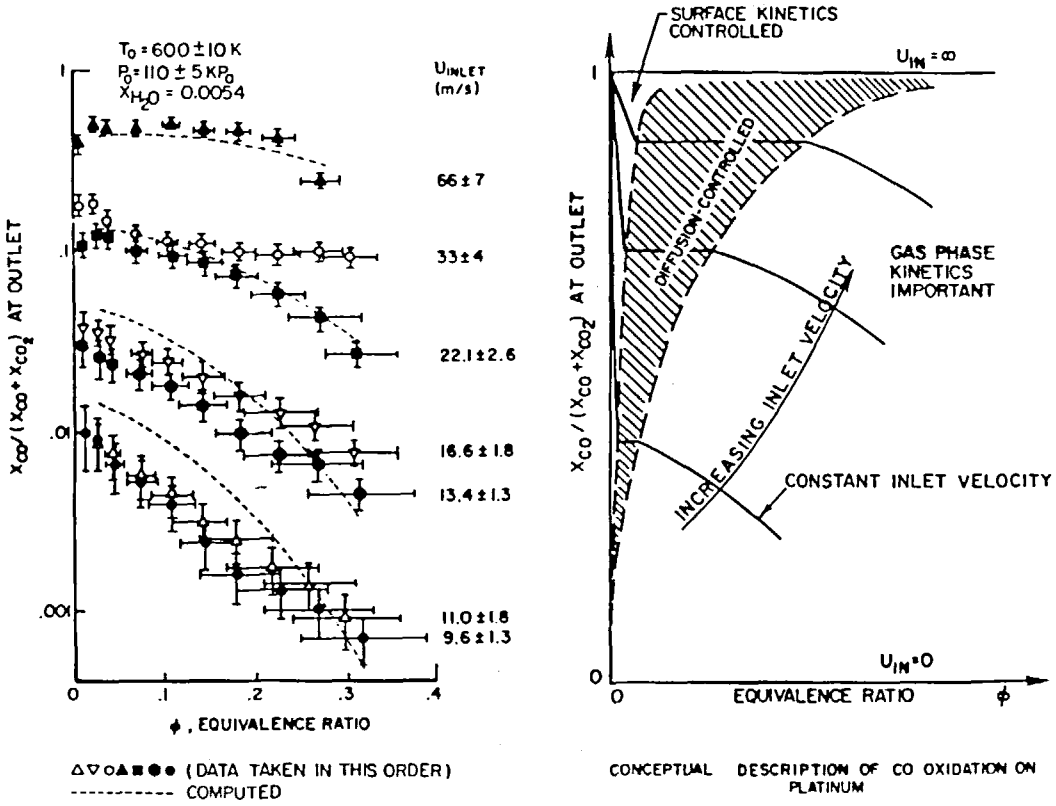

FIG. 6. Measured and computed CO emissions vs equivalence ratio and inlet velocity at specified pressure, inlet temperature and water content.

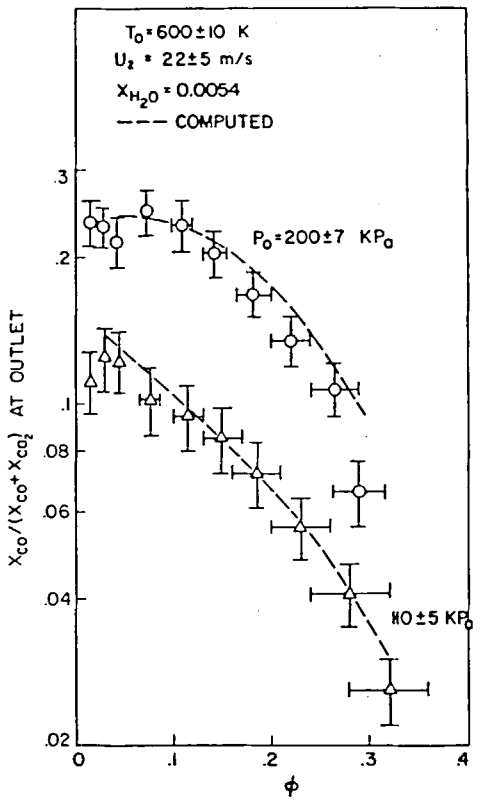

FIG. 7. Fraction of CO unburned vs equivalence ratio and pressure at specified inlet temperature, velocity and water content.

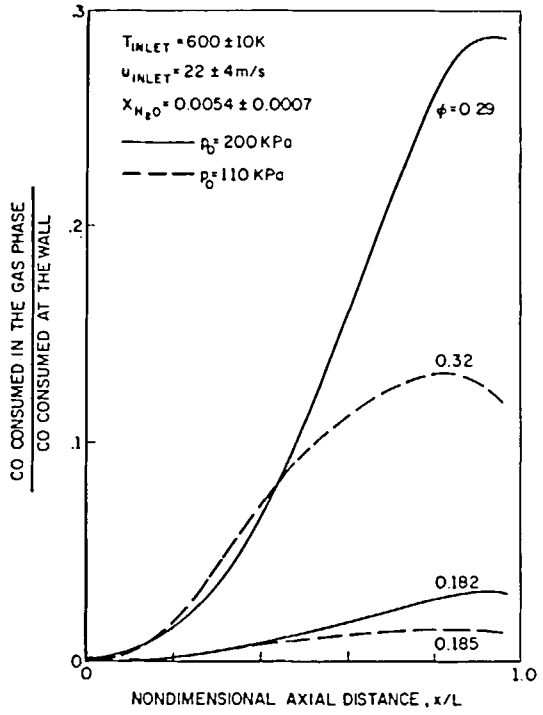

FIG. 8. CO–air oxidation on Pt: computed local gas phase vs surface contribution-effect of ϕ and pressure.

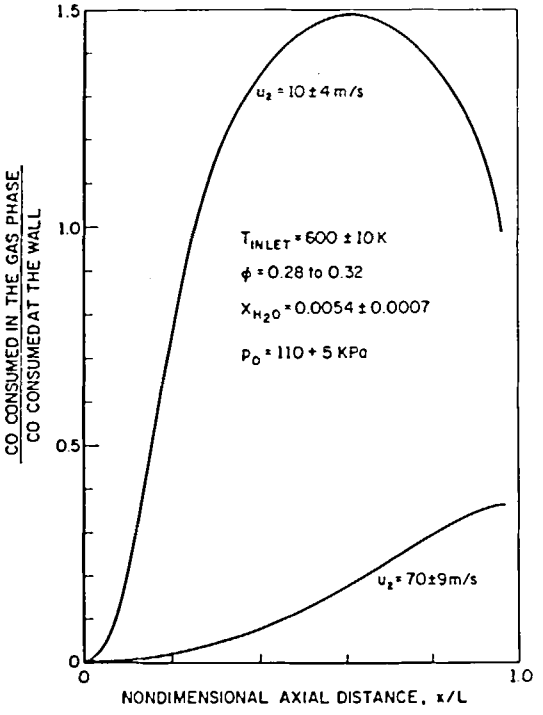

FIG. 9. CO–air oxidation on Pt: computed local gas phase vs surface contribution-effect of velocity.

the diffusion coefficients are inversely proportional to pressure, increasing p from 110 to 200 kPa raises emissions and widens the diffusion-controlled region. For $\phi \geqslant 0.3$, the experimental data show a steeper slope for $p = 200$ kPa than for $p = 110$ kPa. This is the effect of increased gas-phase kinetic rates.

The model underpredicts emissions slightly at larger ϕ and for longer residence times, i.e. where gas-phase kinetics contributes substantially to CO conversion. It is possible that the overall, one-step CO oxidation rate of Howard *et al* [39], proposed for CO–air lean mixtures at $p = 1$ atm., is less accurate at higher pressure and larger ϕ.

Given the reasonable matching of computed and measured data, it is useful to look at the predicted ratio between CO oxidized in the gas phase and CO oxidized at the catalytic wall (Figs. 8–11).

Figures 8 and 9 show that the gas phase becomes important for CO conversion toward the outlet of the channel, where the temperature is higher. They also indicate that for large ϕ, pressure, or residence time the axial station at which homogeneous reactions become important tends to move closer to the entrance.

Figures 8 and 9 also show that near the exit homogeneous conversion rates decrease more rapidly than heterogeneous ones. Both homogeneous and heterogeneous rates decrease on account of decreasing CO concentration and decreasing wall (Fig. 5) and gas temperatures. Both rates decrease as [CO], but homogeneous rates decrease exponentially with temperature, whereas heterogeneous rates decrease only as $T^{1.5}$ [due to equation (2) and to the diffusion-controlled nature of the heterogeneous conversion].

When the contribution of gas phase and surface to

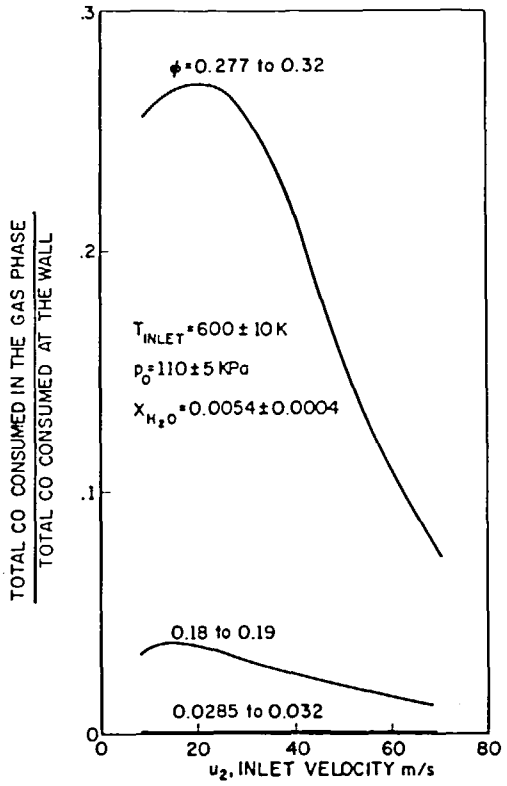

FIG. 10. CO-air oxidation on Pt: computed local gas phase vs surface contribution-effect of ϕ and pressure.

the CO conversion are integrated over the entire channel, the model indicates that most CO is oxidized at the surface. However, Figs. 10 and 11 show the large effects of residence time and pressure at larger ϕ, and, therefore, the importance of gas-phase reactions in this region. For small ϕ and at shorter residence times, the results of the model become insensitive to the presence of gas-phase kinetics, in accordance with the experiments.

The apparent contradiction between the observation of higher unburnt CO and same substrate temperature for the high pressures and high velocity cases is due to the fact that mass and heat transfer rates are comparable for the gas mixture tested (Lewis number $\approx$ unity). Thus the wall temperature in a diffusion-dominated regime depends on ϕ only. While higher pressure reduces the diffusional mass transfer and would tend to reduce the substrate temperature, it also reduces the thermal diffusivity of the gas, which tends to increase the wall temperature. In contradistinction, CO emissions depend on pressure, since a reduction in the CO mass transfer rate to the catalytic wall at higher pressures results automatically in more CO in the exhaust.

4.2. CO–*inert*–O_2 *mixtures*

To study the effect of diffusion on CO conversion a total of 51 runs were performed with fuel-oxidizer combinations in which air was replaced by mixtures of an inert (N_2, CO_2, He, Ar) and O_2. The experimental procedure consisted of bringing the temperature of the test section and connected hardware to the desired steady-state conditions with air, and then injecting the CO–inert–O_2 mixtures. The parameters and conditions kept fixed are summarized in Table 2. A change of the inert gas affects mass and heat diffusion and final combustion temperature through the change in the specific heat of the mixture.

The influence of mass diffusion can be estimated in terms of the binary diffusion coefficient of CO into N_2, CO_2, Ar, He, since the mass fraction of the inert dominates. The combined effect of mass diffusion and heat transfer is shown by the Lewis number of the mixture, defined as $Le = \lambda/C_p\rho D_{1,2}$ where $1 \equiv$ CO and $2 \equiv$ inert. Finally, the effect of the inert on the wall temperature may be estimated by calculating the adiabatic flame temperature with the different inert gases. The results are summarized in Table 3.

From the comparison of these three effects, it is clear

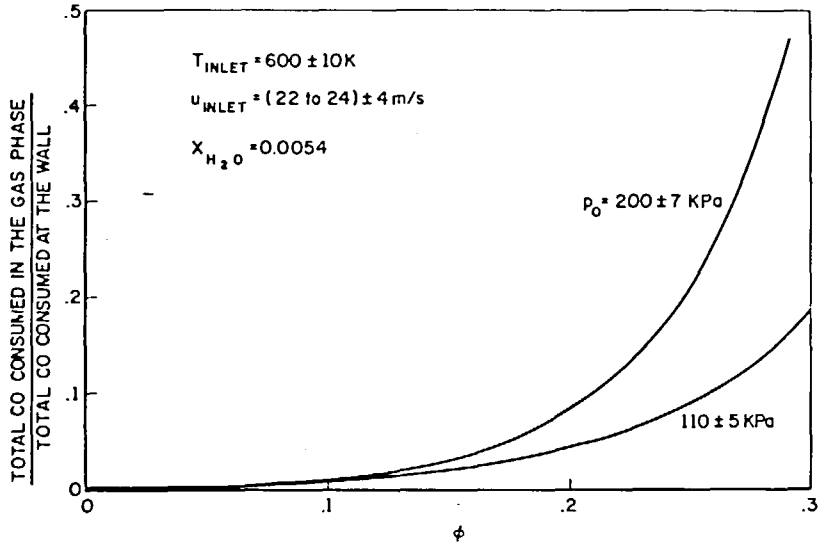

FIG. 11. CO-air oxidation on Pt: computed local gas phase vs surface contribution-effect of ϕ and pressure.

Table 2

Inert gas	Ar	He	N_2	CO_2
Inlet pressure	110±4	110±4	110±4	110±4 kPa
Inlet temperature	600±10	700±20	700±10	690±14 K
Inlet velocity	11±6	13±7	13±5	13±4 m s^{-1}
Equivalence ratio	0.013–0.29	0.022–0.25	0.024–0.38	0.03–0.56

that while mass diffusion is progressively faster in CO_2, N_2, Ar, and He, thermal diffusion increases even more markedly, as shown by the increasing Lewis number. Thus one would have expected a decreasing wall temperature whereas the measured one shown in Fig. 12 generally increases in better correlation with the adiabatic flame temperature in the gas that reflects the effect of the mixture specific heat. Perhaps the above global estimates are not sufficient to characterize the outcome of the complex, spatially non-uniform, strongly coupled processes that were demonstrated to occur within the monolith. Complex trends are also exhibited by the CO emissions that are discussed next.

CO conversion is illustrated in Figs. 13 and 14 for the four inert gases and vs equivalence ratio. Changing inert gases, at constant ϕ, emissions decrease with increasing adiabatic flame temperature. But for a given inert, as ϕ increases emissions do not decrease as simply as for the CO–air mixtures of Fig. 6.

When comparing runs with N_2 as inert (Figs. 12 and 13) to the runs with air (Figs. 5 and 6) under the same conditions one notices: (1) with N_2, CO emissions are about one to two orders of magnitude higher; (2) they increase with ϕ; and (3) the substrate temperature is approximately the same for the same ϕ.

Table 3

Inert	$D_{1,2}/D_{1,N_2}$	*Le*	$T^*_{w\,meas.}$	$T^*_{adiabatic\ flame}$
CO_2	0.86	0.7	1000	1025
N_2	1.00	1.0	1200	1200
Ar	1.03	1.6	1280	1280
He	2.84	1.3	1420	1380

* at $\phi = 0.20$.

The last observation cannot be readily explained, as already discussed, and the first two are also puzzling. Detailed computations were performed and all underpredicted significantly the amount of the measured emissions.

Degradation of the catalyst was suspected but not considered likely, since the runs with CO–N_2–O_2 were performed immediately after the runs with CO–air. The only difference between the two series appears to be the water content of the inlet gas. In the CO–air series the H_2O molar fraction was 0.0054. In the CO–inert–O_2

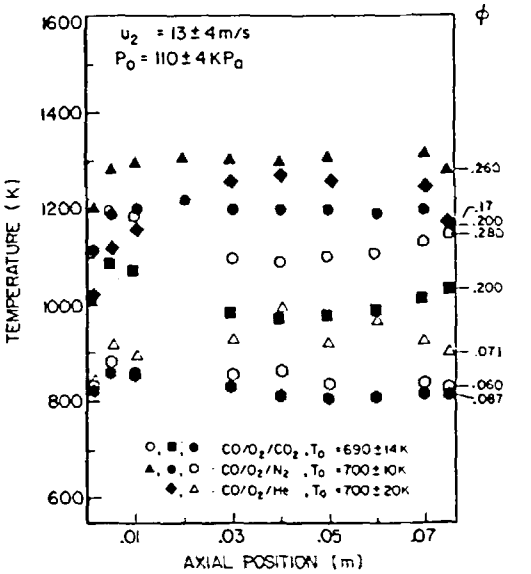

FIG. 12. Substrate temperature vs axial distance for CO–O_2–CO_2, CO–O_2–N_2 and CO–O_2–He at specified inlet temperatures, velocities, pressure and equivalence ratios.

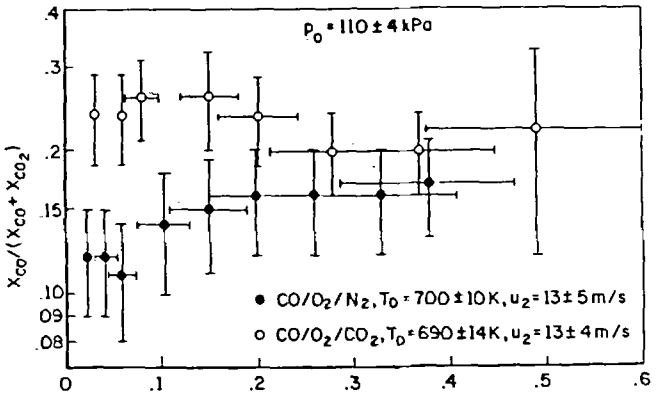

FIG. 13. CO–O_2–N_2 and CO–O_2–CO_2 mixtures: measured fraction of unburned CO vs equivalence ratio at specified inlet temperatures, pressures and velocities.

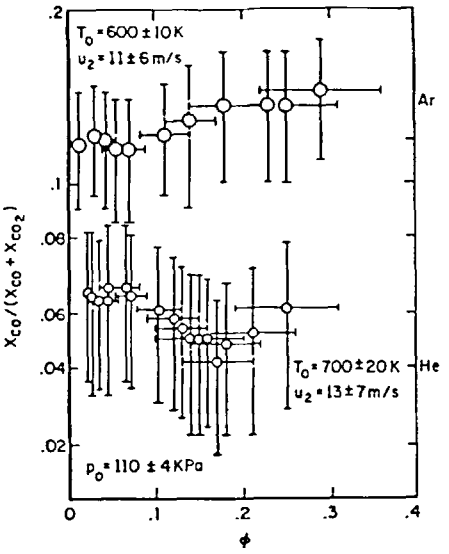

FIG. 14. CO–O_2–Ar and CO–O_2–He mixtures: measured fraction of unburned CO vs equivalence ratio at specified inlet temperatures, pressures and velocities.

series the water content was determined by the H_2O present in the gas bottles, typically a few ppm, and by the residual water left in the test rig by the preheating with air. No reliable measurements of H_2O were taken (due to the hygrometer characteristics) but for CO–N_2–O_2 the H_2O molar fraction at the hygrometer station decreased from 0.002 to 0.0004 during consecutive runs, while ϕ was increased. The gradual flushing out of H_2O while taking the data with dry mixtures parallels the increase of emissions with increasing ϕ.

The computations for the CO–air cases showed that at low velocity and high ϕ the gas phase conversion can account for as much as 20% of the total (Fig. 10). Thus, if homogeneous conversion is totally suppressed in the absence of H_2O, the measured 16% CO emissions of Fig. 13 at $\phi \approx 0.3$ could possibly be explained, as could the increasing emissions with increasing ϕ. However, the lack of homogeneous oxidation leaves more CO in the gas, radial gradients and diffusion rates become larger, and more CO is oxidized at the wall. Indeed computations without homogeneous reactions showed increased emissions but not in the large amounts that were measured. Besides, for $\phi < 0.1$, homogeneous contributions are predicted to be negligible while emissions are still much higher than for the CO–air case. Thus, if sudden degradation of the catalyst, or other unknown experimental errors, are excluded one would conclude that H_2O affects also the high-temperature catalytic oxidation of CO on platinum. Due to the importance of this possibility, additional experiments were later performed with CO–air mixtures in which the water content of the inlet stream was precisely measured by a Dupont 510 Moisture Analyzer and determined to be of order 10, 100, and 1000 ppm in different cases. No effect of the water content on emission of CO was found for $0.03 \leqslant \phi \leqslant 0.23$. (These data have not been formally reported but can be found in ref. [41].) However, we cannot prove that the monolith itself contained no absorbed water during these tests. Thus the possibility of H_2O effects on the catalytic oxidation of CO on platinum at high temperature still exists and some speculations about it are put forth below.

It is known that gas phase oxidation of CO requires OH radicals [39, 42]. It is conceivable that *at high temperature* the conventional CO oxidation mechanism on Pt, proceeding via chemisorption of either or both CO and O_2 [43–45], gives way to a different mechanism in which OH radicals produced at the platinum surface from H_2O, attack the CO molecules in a thin gas-layer adjacent to the catalyst, thus actually simulating heterogeneous oxidation. It is also interesting that high-temperature OH desorption from Pt has been proposed as a 'clean' source of OH for chemical kinetics studies [46, 47]. Low pressure studies indicate that OH escapes the platinum surface only above a temperature ~800 K [48]; preliminary results obtained by Dryer [49] using detailed kinetics for CO–air mixtures at atmospheric pressure indicate that H_2O_2 and HO_2, present in finite amounts in the same temperature range, are good candidates as species easily decomposed by Pt to form OH.

Finally catalytic processes generating radicals have been observed before. The term 'heterohomogeneous catalysis' has been coined to describe them [50].

5. CONCLUSIONS

Catalytic oxidation of CO in air and in inert–O_2 mixtures over a platinum monolithic catalyst has been investigated over a wide range of flow velocities and equivalence ratios and at different pressures. Under the tested conditions, oxidation proceeds in a diffusion-controlled regime and gas-phase chemical reactions become important only for the lowest velocities and highest equivalence ratios.

There is the possibility that the presence of water increases the catalytic oxidation rate of CO. If so, OH radicals generated at high temperature at the platinum surface in the presence of water could be responsible for it.

Acknowledgements—This research was supported by the Air Force Office of Scientific Research under Grant No. AFOSR-76-3052 (Dr B. T. Wolfson, Grant Monitor); by the Department of Energy under Contract No. DE-AC21-80MC14035 (Mr V. Kothari, Technical Project Officer), and by NASA-Lewis Research Center (Dr Andrew Szaniszlo, Grant Monitor). The authors are indebted to Dr W. C. Pfefferle for his many valuable suggestions.

REFERENCES

1. W. S. Blazowski and G. E. Bresowar, Preliminary study of the catalytic combustor concept as applied to aircraft gas turbines, Air Force Appl. Prop. Lab. Tech. Rep. TR-74-32 (1974).
2. T. J. Rosfjord, Catalytic combustion for gas turbine engines, AIAA Pap. 76–46 (1976).
3. V. J. Siminski and H. J. Shaw, Development of a hybrid

catalytic combustor, *Trans. Am. Soc. Mech. Engrs*, Series A, *J. Engng Pwr* **100**, 267–278 (1978).
4. A. J. Szaniszlo, The advanced low-emissions catalytic combustion program Phase I—Description and status, Environ. Prot. Agency, Off. Res. Dev. Rep. 600/7-79-038, pp. 385–402 (1979).
5. L. C. Angello and R. J. Rosfjord, Application of catalytic flame stabilization for aircraft afterburners, Environ. Prot. Agency, Off. Res. Dev. Rep. 600/7-79-038, pp. 61–94 (1979).
6. I. T. Osgerby, R. M. Heck, R. V. Carrubba, C. C. Gleason and E. J. Mularz, Combustion catalyst study for simulated aircraft idle mode operation, Environ. Prot. Agency, Off. Res. Dev. Rep. 600/9-80-035, pp. 398–428 (1980).
7. W. C. Pfefferle, R. V. Carrubba, R. M. Heck and G. W. Roberts, CATHATHERMAL combustion: a new process for low-emissions fuel conversion, Am. Soc. Mech. Eng. Pap. 76-WA/Fu-1 (1975).
8. R. V. Carrubba, M. Chang, W. C. Pfefferle and L. M. Polinski, Catalytically supported combustion for emission control, Spec. Rep.-Electr. Power Res. Inst. (Palo Alto, CA) SR-39, pp. 316–323 (1976).
9. S. M. DeCorso, S. Mumford, R. Carrubba and R. M. Heck, Catalysis for gas combustors, Am. Soc. Mech. Eng. Pap. 76-GT-4 (1976).
10. W. V. Krill and J. P. Kesselring, The development of catalytic combustors for stationary source applications, Environ. Prot. Agency, Off. Res. Dev. Rep. 600/7-79-038, pp. 259–290 (1979).
11. S. M. DeCorso and D. C. Carl, Structural analysis of a preliminary catalytic ceramic design, Environ. Prot. Agency, Off. Res. Dev. Rep. 600/7-79-038, pp. 139–156 (1979).
12. H. Fukuzawa and Y. Ishihara, Catalytic combustion for gas turbines, Environ. Prot. Agency, Off. Res. Dev. Rep. 600/9-80-035, pp. 349–364 (1980).
13. D. N. Anderson, Performance and emissions of a catalytic reseator with propane, diesel and jet A fuels, NASA Tech. Mem. TM-73796 (1977).
14. D. N. Anderson, Effect of catalytic reactor length and cell density on performance, presented at the U.S. Environ. Prot. Agency, Off. Res. Dev., Second Workshop on Catalytic Combustion, Raleigh, NC, 21–22 June (1977).
15. D. N. Anderson, The effect of initial temperature on the performance of a catalytic reactor, NASA Tech. Mem. TM-78977 (1978).
16. D. N. Anderson, Effect of inlet temperature on the performance of a catalytic reactor, Environ. Prot. Agency, Off. Res. Dev. Rep. 600/7-79-038, pp. 403–426 (1979).
17. D. N. Anderson, R. R. Tacina and T. S. Mroz, Catalytic combustion for the automotive gas turbine engine, NASA Tech. Mem. TM X-73589 (1977).
18. R. Carrubba and I. T. Osgerby, Catalyst design studies in low BTU gas combustion, Environ. Prot. Agency, Off. Res. Dev. Rep. 600/7-79-038, pp. 435–436 (1979).
19. J. T. Pogson and M. N. Mansour, No. 6 fuel oil catalytic combustion, Environ. Prot. Agency, Off. Res. Dev. Rep. 600/7-79-038, pp. 111–138 (1979).
20. T. J. Rosfjord, Catalytic combustion of heavy partially vaporized fuels, Environ. Prot. Agency, Off. Res. Dev. Rep. 600/9-80-035, pp. 527–537 (1980).
21. H. Tong, E. K. Chu and G. C. Snow, Catalytic combustion of alternative fuels, Environ. Prot. Agency, Off. Res. Dev. Rep. 600/9-80-035, pp. 490–515 (1980).
22. R. M. Heck, M. Chang, H. Hess and R. Carrubba, Durability testing at one atmosphere of advanced catalysts and catalyst supports for automotive gas turbine engine combustors, NASA Contract. Rep. CR 135132 (1977).
23. R. D. Matthews and R. F. Sawyer, Fuel nitrogen conversion and catalytic combustion, West. Sect. Combust. Inst., Prepr. Pap. 77-40 (1977).
24. E. K. Chu and J. P. Kesselring, Fuel NO_x control by catalytic combustion, Environ. Prot. Agency, Off. Res. Dev. Rep. 600/7-79-038, pp. 291–330 (1979).
25. B. A. Folsom, C. W. Courtney and M. P. Heap, Environmental aspects of low BTU gas-fired catalytic combustion, Environ. Prot. Agency, Off. Res. Dev. Rep. 600/7-79-038, pp. 345–384 (1979).
26. E. K. Chu, Evaluation of a lean catalytic combustion concept for nitrogeneous fuels, Environ. Prot. Agency, Off. Res. Dev. Rep. 600/7-79-038, pp. 538–551 (1980).
27. M. Lavid and F. V. Bracco, A review of boundary layer studies relating to catalytic combustion, Report No. 1282, Dept. of Mech. and Aerosp. Eng., Princeton University (1976).
28. J. T. Kelly, R. M. Kendall, E. Chu and J. P. Kesselring, Development and application of the PROF-HET catalytic combustion code, West. Sect. Combust. Inst., Prepr. Pap. 77–33 (1977).
29. W. C. Pfefferle, The catalytic combustor: an approach to cleaner combustion, *J. Energy* **2**, 142–146 (1978).
30. A. E. Cerkanowicz, R. B. Cole and J. G. Stevens, Catalytic combustion modeling: Comparisons with experimental data, *Trans. Am. Soc. Mech. Engrs*, Series A, *J. Engng Pwr* **99**, 593–600 (1977).
31. J. P. Kesselring, W. V. Krill and R. M. Kendall, Design criteria for stationary source catalytic combustors, West. Sect. Combust. Inst., Prepr. Pap. 77–32 (1977).
32. J. S. T'ien, Catalytic honeycomb combustor: Steady-state model and comparison with experiments, *J. Energy* **5**, 201–207 (1981).
33. R. M. Fristrom, W. H. Avery and C. Grunfelder, Reactions of simple hydrocarbons in flame fronts-microstructure of C_2 hydrocarbon–oxygen flames, in *7th Symp. (Int.) on Combustion*, pp. 304–310. Butterworths, London (1959).
34. L. L. Hegedus, Temperature excursions in catalytic monoliths, *A.I.Ch.E.Jl* **21**, 849–853 (1973).
35. F. V. Bracco, On the optimal utilization of experimental data, *AIAA Jl* **13**, 1421–1422 (1975).
36. F. A. Williams, *Combustion Theory*, pp. 2–4. Addison–Wesley, Reading, MA (1965).
37. A. D. Gosman annd F. J. K. Ideriah, TEACH-T: A general computer program for two-dimensional, turbulent, recirculating flow, Dept. of Mech. Engr., Imperial College, London (1976).
38. A. Murty-Kanury, *Introduction to Combustion Phenomena*, pp. 383–387. Gordon and Breach, New York (1977).
39. J. B. Howard, G. C. Williams and D. H. Fine, Kinetics of carbon monoxide oxidation in postflame gases, in *14th Symp. (Int.) on Combustion*, pp. 975–986. The Comb. Inst., Pittsburgh (1973).
40. S. E. Voltz, C. R. Morgan, D. Liederman and S. M. Jacob, Kinetic study of carbon monoxide and propylene oxidation on platinum catalysts, *Ind. Eng. Chem., Prod. Res. Dev.* **12**, 294–301 (1973).
41. P. M. Curtis, F. V. Bracco and B. S. H. Royce, High temperature catalytically assisted combustion, Mech. and Aerosp. Eng. Dept., Princeton University, Proposal to AFOSR for renewal of Grant 81-0248, January (1982).
42. W. C. Gardiner and D. B. Olson, Chemical kinetics of high temperature combustion, in *Annual Review of Physical Chemistry* (edited by B. S. Rabinovitch, J. M. Schurr and H. L. Strauss), pp. 377–399. Annual Reviews, Palo Alto (1980).
43. T. Engel and G. Ertl, Elementary steps in the catalytic oxidation of carbon monoxide on platinum metals, in *Advances in Catalysis* (edited by D. D. Elay, H. Pines and P. B. Weisz), Vol. 28, pp. 55–59. Academic Press, New York (1979).
44. C. T. Campbell, G. Ertl, H. Kuipers and J. Segner, A molecular beam study of the catalytic oxidation of CO on a Pt (111) surface, *J. Chem. Phys.* **73**, 5862–5873 (1980).
45. J. A. Strozier, Oxidation of CO on Pt by an AC pulsing technique. II Experiment, *Surf. Sci.* **87**, 161–186 (1979).

46. D. E. Tevault, L. D. Talley and M. C. Lin, Matrix isolation and laser diagnostic studies of catalytic oxidation of H_2 and D_2 on platinum, *J. Chem. Phys.* **72**, 3314–3319 (1979).
47. L. D. Talley, W. A. Sanders, D. J. Bogan and M. C. Lin, Internal energy of hydroxyl radicals desorbing from polycrystalline Pt surfaces, *Chem. Phys. Lett.* **78**, 500–503 (1981).
48. L. D. Talley, D. E. Tevault and M. C. Lin, Laser diagnostics of matrix-isolated OH radicals from oxidation of H_2 on platinum, *Chem. Phys. Lett.* **66**, 584–586 (1979).
49. F. Dryer, Presentation at the Army Research Office Workshop on Engine Combustion, Atlanta, GA, 2–3 April (1981).
50. C. N. Satterfield, *Heterogeneous Catalysis in Practice*, pp. 10–11. McGraw-Hill, New York (1980).

COMBUSTION CATALYTIQUE A HAUTE TEMPERATURE DES MELANGES CO-O_2-Na, Ar, He, CO_2-H_2O SUR DU PLATINE

Résumé—Dans un réacteur avec écoulement permanent, utilisant un catalyseur en nid d'abeille recouvert de platine, avec un diamètre de canal de 1,4 mm et une longueur de 76 mm, des mesures de température du substrat sont faites à dix emplacements axiaux, ainsi que des concentrations en sortie de CO, CO_2, O_2 et de chute de pression avec des mélanges CO–air à une température d'entrée de 600 K, des pressions entre 110 et 200 kPa, des vitesses d'entrée entre 10 et 70 m s^{-1}, des rapports d'équivalence entre 0,013 et 0,32 et une composition en eau de 0,54 mol %. On été utilisés aussi des mélanges CO–CO_2, N_2, Ar, He–O_2 à 600–700 K, 110 kPa, 11–13 m s^{-1} et des rapports d'équivalence entre 0,031 et 0,56. L'évolution des gaz dans un canal sont calculés à l'aide d'un modèle bidimensionnel, permanent qui inclut la convection axiale et radiale, la diffusion laminaire de masse, de quantité de mouvement et d'énergie, la réaction irréversible-homogène et initialement une réaction de surface à vitesse finie. La comparaison entre les calculs et les mesures est satisfaisante. Dans les conditions étudiées, l'oxydation de CO est principalement contrôlée par la diffusion. Des réactions homogènes sont importantes seulement pour les plus faibles vitesses et les plus grands rapports d'équivalence. Il semble que la présence d'eau augmente l'oxydation catalytique de CO à haute température.

KATALYTISCHE HOCHTEMPERATURVERBRENNUNG VON CO-O_2-Ar, He, CO_2-H_2O-GEMISCHEN AUF PLATIN

Zusammenfassung—In einem stationären Fließreaktor mit einem wabenförmigen, platinbeschichteten Katalysator mit Kanaldurchmessern von 1,4 mm und einer Länge von 76 mm werden Messungen der Substrattemperatur an 10 axialen Stellen, der Austritts-Konzentrationen von CO, CO_2, O_2 und der Druckverluste von CO–Luft-Gemischen durchgeführt, bei einer Eintrittstemperatur von 600 K, Drücken von 110–200 kPa, Eintrittsgeschwindigkeiten von 10–70 m s^{-1} und Mischungsverhältnissen von 0,013–0,32. Die Gasprozesse innerhalb eines Kanals wurden dann mit einem zweidimensionalen Modell berechnet, wobei axiale und radiale Konvektion, laminare Diffusion von Masse, Impuls und Energie, eine homogene einstufige irreversible Reaktion und zu Anfang eine Oberflächenreaktion endlicher Geschwindigkeit berücksichtigt wurden. Der Vergleich von berechneten und gemessenen Größen war befriedigend. Unter den Testbedingungen verläuft die Oxidation von CO meistens diffusionsbestimmt. Homogene Reaktionen sind nur bei den niedrigsten Geschwindigkeiten und höchsten Mischungsverhältnissen von Bedeutung. Es scheint, daß die Anwesenheit von Wasser die Geschwindigkeit der katalytischen Hochtemperaturoxidation von CO erhöht.

ВЫСОКОТЕМПЕРАТУРНОЕ КАТАЛИТИЧЕСКОЕ ГОРЕНИЕ СМЕСЕЙ CO-O_2-N_2, Ar, He, CO_2-H_2O НА ПЛАТИНОВОЙ ПОВЕРХНОСТИ

Аннотация—В реакторе со стационарным режимом течения, в котором используется покрытый платиной сотовый катализатор с диаметром каналов 1,4 мм и длиной 76 мм, проведены измерения температуры подложки в трех аксиальных точках, концентраций CO, CO_2 и O_2 на выходе, а также перепадов давления в смесях CO с воздухом при температуре на входе 600 К, давлениях 110-200 кн/м^2, скоростях на входе 10–70 м/сек, отношениях компонентов смеси 0,013–0,32 и содержании воды 0,54 мол %. Также исследовались смеси CO–CO_2, $И_2$, Ar, He–O_2 при 600–700 К, 110 кн/м^2, 11–13 м/сек и соотношениях компонентов в диапазоне 0,031–0,56. Процессы, происходящие в газовой среде внутри канала, рассчитывались с помощью двумерной стационарной модели, учитывающей осевую и радиальную конвекцию, ламинарную диффузию массы, импульса и энергии, однородную одноступенчатую необратимую реакцию и, на первом этапе, поверхностную реакцию, протекающую с конечной скоростью. Получено удовлетворительное совпадение расчетных и измеренных величин. В исследуемых условиях насыщение CO кислородом происходит в основном за счет диффузии. Гомогенные реакции имеют существенное значение только при самых малых скоростях течения и очень больших величинах соотношения компонент. По-видимому, увеличение скорости каталитического окисления CO при высокой температуре происходит из-за наличия в смеси воды.